energy&fuels

Article

pubs.acs.org/EF

Pyrolysis of Kerogen of Bazhenov Shale: Kinetics and Influence of Inherent Pyrite

Andrey Galukhin,* Alexander Gerasimov, Ilya Nikolaev, Roman Nosov, and Yuri Osin

Kazan Federal University, 18 Kremlevskaya Street, Kazan 420008, Russian Federation

ABSTRACT: In the present study, we investigated in detail the influence of the depyritization procedure on the structure and morphology of the organic matter of Bazhenov shale. We monitored both structural and morphological properties of the organic matter of shale during chemical treatment by a complex of physical methods, including different types of spectroscopies, scanning electron microscopy, and physisorption analysis. We also applied non-istothermal kinetic analysis to study the effect of inherent pyrite on the pyrolysis of kerogen in a wide temperature range and showed that the presence of inherent pyrite has no impact on the pyrolysis process.

1. INTRODUCTION

The increasing consumption of the energy resources accompanied by a shortage of the conventional oil reserves motivates us to search for alternative sources of liquid hydrocarbons. One of the most promising sources of hydrocarbons is organic matter of shales, consisting of shale oil and shale kerogen. According to the International Energy Agency, these reserves contain more than 1 trillion barrels of technically recoverable oil.[1] Besides shale oil, significant attention of scientists is focused on *in situ* generation of synthetic oil from kerogen contained in shale deposits. This process demands high temperatures (>350 °C), which can be reached, for instance, in the pyrolysis front during *in situ* combustion[2] or during the *in situ* conversion process of Shell, with the latter being specially designed to convert kerogen in oil shale to shale oil.[3]

A lot of studies related to pyrolysis of shale were conducted on the basis of native,[4−7] full and partially demineralized core samples.[8−10] Among all minerals presented in shale, the influence of pyrite on organic matter transformation is most poorly studied. There exist only few works related to the effect of pyrite on kerogen pyrolysis. For instance, the effect of inherent and additional pyrite on oil shale pyrolysis was investigated in a fixed-bed reactor.[11] The results show that inherent pyrite can improve the oil yield, whereas additional pyrite increases the amount of volatiles. Moreover, the influence of pyrite depends upon the maturity of the organic matter:[12] according to electron spin resonance spectroscopy measurements, pyrite shows a pronounced effect on the activity of free radicals of kerogen samples representing the diagenesis stage. The authors proposed a possible mechanism of the action of pyrite: elemental sulfur formed during pyrite decomposition acts like a hydrogen atom acceptor.

However, we mention that commonly used chemical treatments, applied for pyrite removal, such as dilute nitric acid, lithium aluminum hydride, and sodium borohydride, cause significant chemical changes of the organic matter in the residual kerogen.[13,14] Most of the studies published in this field ignore the changes in organic matter taking place during pyrite removal and related changes in the reactivity of kerogen.

In the present study, we profoundly investigated the influence of the chosen demineralization process on the structure and morphology of the kerogen of Bazhenov shale and applied non-istothermal kinetic analysis to study the effect of inherent pyrite on the pyrolysis of kerogen.

2. MATERIALS AND METHODS

2.1. Kerogen Sample. The shale rock samples used in this research were obtained from Bazhenov shale (West Siberian Basin, Russia). The organic matter of the Bazhenov Formation originates from plankton and bacteria. The insoluble part of organic matter is presented by type-II kerogen that usually contains 7−8.5% hydrogen and is strongly oil-prone.[15] The geological age of the Bazhenov Formation is a latter part of early Tithonian and an early part of early Berriasian.[16]

Organic solvents, such as trichloromethane and ethanol (purity of all solvents was no less than 99.5%), and inorganic chemicals, such as hydrochloric and hydrofluoric acids, were purchased from Component-Reaktiv and used without additional purification. Chromium(II) chloride (purity of 99.99%) was purchased from Sigma-Aldrich.

2.2. Sample Preparation. The native core was crushed and sieved to a size of <0.50 mm. Then, the sample was extracted by trichloromethane in a Soxhlet extractor to remove oil contained in it. The obtained sample was demineralized by the sequential washing with hydrochloric and hydrofluoric acids. Hydrochloric acid treatment removes carbonates and sulfates, while hydrofluoric acid allows us to purify kerogen from silicates. The kerogen sample was filtered off, washed with distilled water, and dried at 100 °C under reduced pressure (20 mbar). The obtained kerogen sample containing pyrite is denoted as "KerPyr" throughout the text. For the removal of pyrite from kerogen, the following procedure was applied. A total of 2 g of kerogen was added to a solution of chromium(II) chloride (5 g, 0.041 mmol) in 100 mL of ethanol in a three-neck round-bottom flask equipped by a condenser and a dropping funnel filled with 40 mL of concentrated hydrochloric acid. The resulting mixture was refluxed for 2 h, and nitrogen flow was used for hydrogen sulfide removal. A more detailed description of the applied procedure is presented in ref 17. The free kerogen sample is denoted as "Ker" throughout the text.

2.3. Thermal Analysis. Thermogravimetry−differential scanning calorimetry (TG−DSC) experiments of solid samples with mass

Received: February 28, 2017
Revised: May 17, 2017
Published: June 21, 2017

DOI: 10.1021/acs.energyfuels.7b00610
Energy Fuels 2017, 31, 6777−6781

spectrometric (MS) evolved gas analysis were performed using thermoanalyzer STA 449 C Jupiter (Netzsch) coupled with quadrupolar mass spectrometer QMS 403 C Aeolos in the temperature range of 30−600 °C. The experiments were conducted at linear heating rates of 5, 10, 15, and 20 °C/min for kinetic analysis of kerogen samples under argon flow (75 mL/min). An average sample was 10 mg for each run. The obtained DSC curves were processed by Proteus Analysis (version 5.2.1), Netzsch Peak Separation (version 2010.09), and Netzsch Thermokinetics 3.1 (version 06.08.2014) program packs.

2.4. Elemental Analysis. CHNS elemental analysis of kerogen samples was carried out on a PerkinElmer 2400 Series II elemental analyzer. The iron content in the samples was determined by X-ray fluorescence spectroscopy by a Clever C31 instrument (ELERAN).

2.5. X-ray Powder Diffraction (XRPD). XRPD studies were made using a MiniFlex 600 diffractometer (Rigaku) equipped with a D/teX Ultra detector. Cu $K\alpha_1$ radiation (40 kV and 15 mA) was used, and data were collected at 25 °C in the range of 2θ from 2° to 100° with a step of 0.02° and exposure time at each point of 0.24 s without sample rotation.

2.6. Infrared (IR) Spectroscopy. Data were collected using a Bruker Vertex 70 FTIR spectrometer with a single reflection, germanium crystal attenuated total reflection (ATR) accessory (MIRacle, PIKE Technologies). The interferograms were recorded with a resolution of 2 cm^{-1} and 128 scans and Fourier-transformed using a Blackman−Harris apodization function.

2.7. Nuclear Magnetic Resonance (NMR) Spectroscopy. Solid-state cross-polarization magic angle spinning carbon-13 nuclear magnetic resonance (CP/MAS ^{13}C NMR) spectra were recordered on an AVANCE III 400 MHz NMR spectrometer.

2.8. Scanning Electron Microscopy (SEM) and Energy-Dispersive X-ray (EDX) Spectroscopy. SEM measurements and EDX analysis were carried out using a field-emission high-resolution scanning electron microscope Merlin Carl Zeiss equipped with an energy-dispersive spectrometer AZtec X-MAX. Observation photos of the morphology surface were obtained at an accelerating voltage of incident electron of 15 kV and a current probe of 300 pA. During the elemental analysis of the surface, the accelerating voltage of incident electron was 5 kV and the working distance was 9 mm. The probing depth was about 1 μm.

2.9. Brunauer−Emmett−Teller (BET) Surface Area and Porosity Measurements. The BET surface area of kerogen samples was measured by nitrogen adsorption at 77 K with an ASAP 2020 MP (Micromeritics) instrument. About 0.5 g of sample was degassed by heating at 200 °C under vacuum (8 μmHg) for 2 h. The specific surface area (SSA) for each sample was determined by applying the BET equation.

3. RESULTS AND DISCUSSION

3.1. Kerogen Characterization. Prior to investigation of the influence of inherent pyrite on kerogen pyrolysis kinetics, it is necessary to obtain pyrite-free kerogen samples. We applied the chromium(II) chloride method to remove pyrite from kerogen. This method removes pyrite in mild conditions with minimal modification of organic matter.[17] Chromium(II)

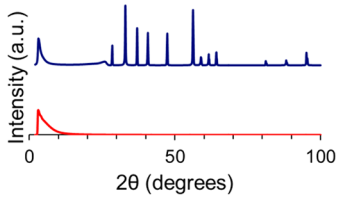

Figure 1. XRPD analysis of kerogen samples before (blue) and after (red) pyrite removal.

Table 1. Kerogen Composition before and after Pyrite Removal (wt %)

sample	C	H	N	S_{tot}	S_{org}	S_p	Fe	pyrite
KerPyr	59.7	3.1	0.4	8.1	2.2	5.9	5.1	11.0
Ker	87.3	6.8	0.0	0.2	0.2	0.0	0.0	0.0

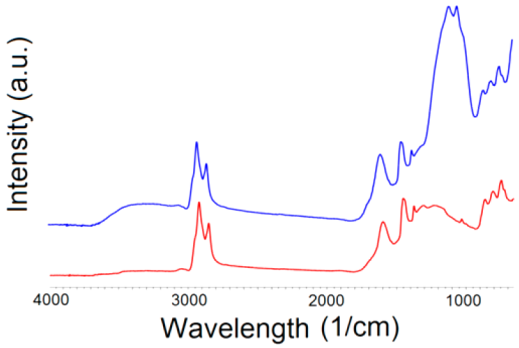

Figure 2. IR spectra of kerogen samples before (blue) and after (red) pyrite removal.

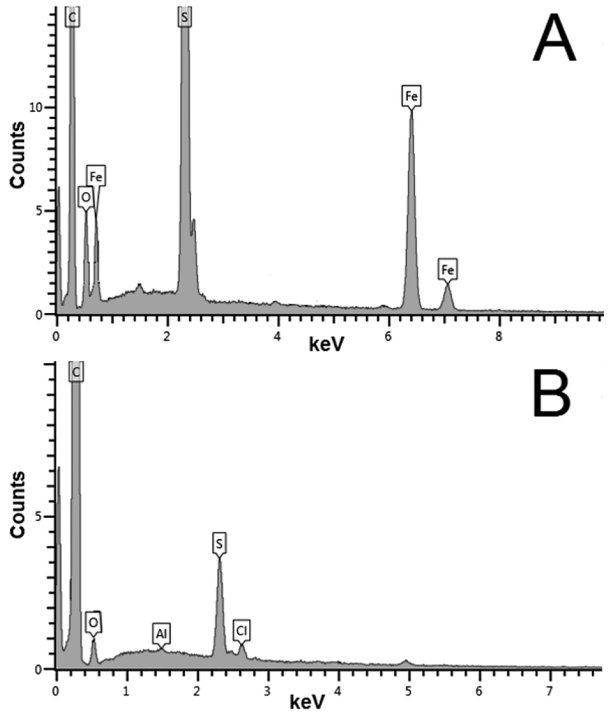

Figure 3. EDX spectra of kerogen samples (A) before and (B) after pyrite removal.

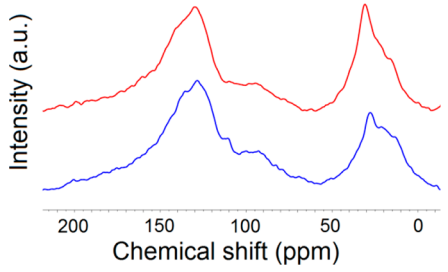

Figure 4. CP/MAS ^{13}C NMR spectra of kerogen samples before (blue) and after (red) pyrite removal.

DOI: 10.1021/acs.energyfuels.7b00610
Energy Fuels 2017, 31, 6777−6781

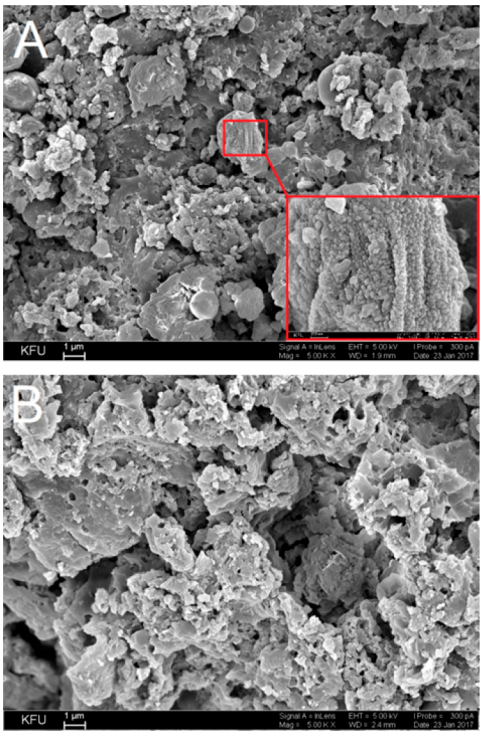

Figure 5. SEM images of the samples (A) before and (B) after pyrite removal. Scale bars are 1 μm and 200 nm (inset).

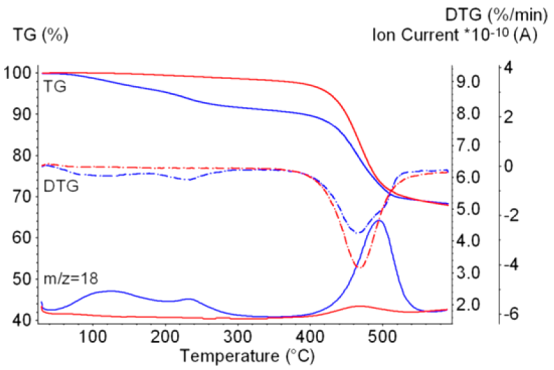

Figure 6. TG, DTG, and selected ion (m/z 18) current curves of KerPyr (blue) and Ker (red) samples obtained at 10 °C/min.

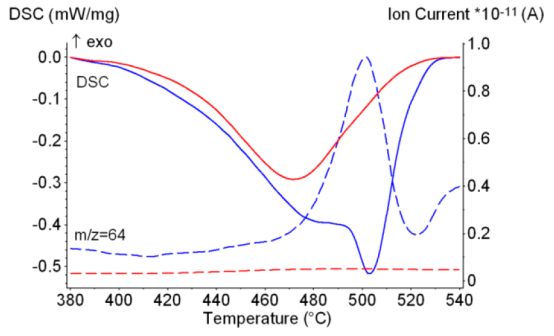

Figure 7. DSC and selected ion current (m/z 64) curves of KerPyr (blue) and Ker (red) samples obtained at 10 °C/min.

chloride reduces pyrite to hydrogen sulfide according to the following reaction:

$$FeS_2 + 2CrCl_2 + 4HCl = FeCl_2 + 2CrCl_3 + H_2S$$

Table 2. DSC Reaction Intervals

	sample	
	KerPyr	Ker
β (°C/min)	interval (°C)	interval (°C)
5	425−510	414−502
10	428−520	425−520
15	434−532	435−520
20	446−541	436−526

We control the degree of pyrite removal by XRPD analysis. Figure 1 shows that chromium(II) chloride treatment leads to complete removal of pyrite. Elemental compositions of both samples are presented in Table 1.

We applied IR spectroscopy to evaluate changes of organic matter after chemical treatment. IR spectra presented on Figure 2 show adsorption bands related to organic matter and corresponding to asymmetric and symmetric vibrations of aliphatic C−H bonds (2922 and 2852 cm^{-1}), stretching of aromatic C−C bonds (1459 and 1595 cm^{-1}), and out-of-plane bending of aromatic C−H bonds (863, 805, and 744 cm^{-1}), which are almost identical for both samples. The only differences that occurred are related to regions of 1050−1100 and 3100−3600 cm^{-1}. We assume differences of obtained IR spectra in a region of 3100−3600 cm^{-1} are due to physically and chemically adsorbed water. This suggestion was proven further by TG−DSC−MS experiments. Intensive adsorption bands at 1100 and 1050 cm^{-1} in the case of sample KerPyr indicate partial oxidation of the pyrite surface.[18,19]

Elemental analysis of the surfaces of the samples by EDX spectroscopy (Figure 3) also confirmed the presence of the increased amount of oxygen atoms on the surface of the sample KerPyr.

Because IR spectroscopy gives information on both organic and inorganic parts of the samples, we additionally applied CP/MAS ^{13}C NMR to confirm that the depyritization procedure does not change the kerogen structure. That method is straightforward non-destructive techniques that can provide useful information about the chemical nature of kerogen.[20] As seen in Figure 4, obtained spectra have two main broad signals corresponding to aliphatic and aromatic carbon. Both spectra have insignificant differences; therefore, we can conclude that organic matter remains unchanged after treatment.

Finally, we studied the morphology of the samples. We applied SEM to study the influence of chemical treatment on the morphology of the kerogen. Figure 5 shows SEM images of the samples KerPyr and Ker. It can be clearly seen that the untreated sample KerPyr (Figure 5A) contains pyrite grains presented by polycrystalline particles (inset of Figure 5A), which are absent in the case of the chemically treated sample Ker (Figure 5B).

BET surface area measurements also show insignificant change of the SSA for samples KerPyr and Ker, which are 9.39 ± 0.06 and 10.63 ± 0.07 m^2/g, respectively. We assume that a slight increase of the SSA of kerogen after pyrite removal is related to kerogen possessing a much greater value of SSA than pyrite.[21] With that taken into account, the rise in the SSA value of the sample after pyrite removal is perfectly explained by the increase of the kerogen percentage from 89 to 100% (Table 1). At the same time, the mesoporosity increases from 0.03 to 0.06 cm^3/g after pyrite removal. Thus, we can conclude that the applied depyritization procedure causes insignificant changes of

DOI: 10.1021/acs.energyfuels.7b00610
Energy Fuels 2017, 31, 6777−6781

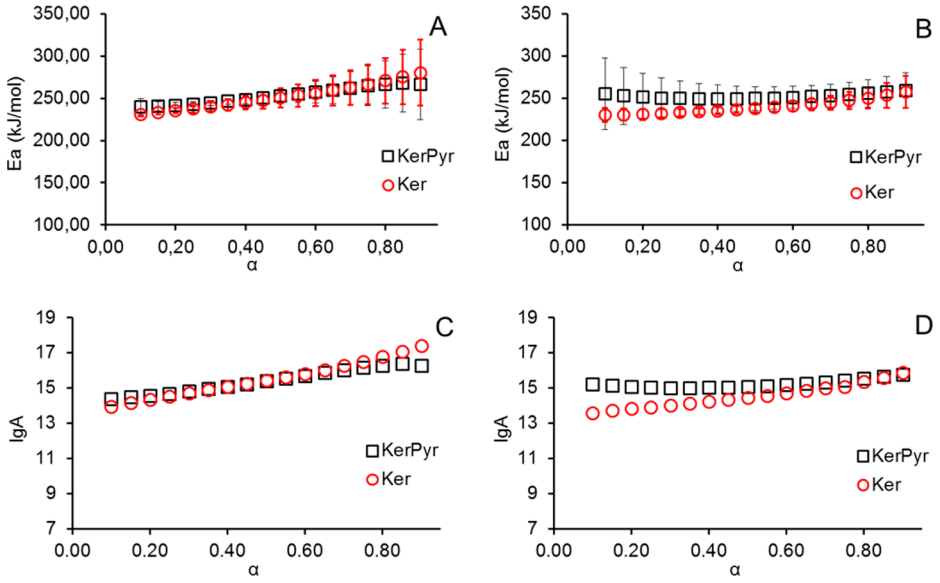

Figure 8. Effective activation energy and pre-exponential factor variations with the extent of conversion calculated by (A and C) Friedman and (B and D) OFW methods.

both the structure and morphology of the organic matter of shale.

3.2. Thermal Analysis Results and Pyrolysis Kinetic Studies. TG and DSC are two of the most popular techniques widely applied in the studies of thermal characteristics of fossil fuels.[22−25] In the current study, we applied TG−DSC analysis coupled with MS to investigate in detail the influence of pyrite on the pyrolysis of kerogen. Figure 6 shows TG and differential thermogravimetry (DTG) curves of samples KerPyr (blue) and Ker (red). It can be clearly seen that the sample KerPyr losses a significant part of its mass (8.31%) during heating to 300 °C, unlike the pyrite-free sample Ker (mass loss is 1.31%). We think that this behavior is related to physically and chemically adsorbed water on the pyrite surface. This suggestion was proven by MS analysis of effluent gases. The ion current curve for m/z 18 (water) peaks at the same temperature values as the DTG curve.

Pyrolysis itself proceeds at the temperature range of 400−550 °C, where the main mass loss occurred; therefore, further studies will be related to this region. Figure 7 shows DSC curves of samples KerPyr and Ker: in case of the first sample, two overlapping endothermic peaks occur.

These peaks correspond to decomposition of kerogen (broad peak) and pyrite (narrow peak). The narrow peak appearance coincides with evolution of the product with m/z 64 (blue dashed line in Figure 7). It should be noted that this mass-to-charge ratio can be related to both sulfur dioxide (SO_2) and dimeric sulfur (S_2). In this study, we assigned it to S_2 released during pyrite decomposition according to the following equation:[26]

$$(1 - x)FeS_{2(s)} = Fe_{(1-x)}S_{(s)} + (0.5 - x)S_{2(g)}$$

Thermal analysis is widely applied for investigation of kinetics of the pyrolysis process.[27,28] We applied non-isothermal kinetic analysis based on an isoconversional approach[29] to study kinetics of pyrolysis of the kerogen. According to this approach, the rate of thermally stimulated processes proceeding in the condensed phase can be described as a function of the absolute temperature (T) and the extent of conversion (α) (eq 1).

$$\frac{d\alpha}{dt} = k(T)f(\alpha) \quad (1)$$

The isoconversional principle states that the reaction rate at a constant extent of conversion only depends upon the temperature. This statement allows us to remove the reaction model from kinetic computations (eq 2).

$$\left[\frac{\partial \ln\left(\frac{d\alpha}{dt}\right)}{\partial T^{-1}}\right]_{\alpha} = \left[\frac{\partial \ln k(T)}{\partial T^{-1}}\right]_{\alpha} \quad (2)$$

The conversion degree α in DSC is calculated according to eq 3.

$$\alpha = \frac{\int_{t_0}^{t}(dH/dt)dt}{\int_{t_0}^{t_f}(dH/dt)dt} \quad (3)$$

The rate constant $k(T)$ is assumed to obey the Arrhenius law (eq 4).

$$k(T) = Ae^{-E/RT} \quad (4)$$

In this study, we apply two methods to DSC data, which are the integral Ozawa−Flynn−Wall (OFW) method[30,31] and the differential Friedman method.[32] These methods are standard benchmarks allowing us to calculate effective kinetic parameters of thermally stimulated processes. DSC reaction intervals of both samples are grouped in Table 2. We applied a peak separation procedure to resolve DSC peaks in the case of the sample KerPyr.

Figure 8 shows variations of kinetic parameters with the extent of conversion α calculated by two aforementioned isoconversional methods. As seen, the presence of pyrite shows no influence on the pyrolysis process: effective kinetic parameters obtained by two methods almost coincide for both experiments at any extent of conversion.

The median values of effective kinetic parameters calculated by the Friedman method are 252.8 ± 8.1 kJ/mol (log A = 15.40) and 250.3 ± 11.4 kJ/mol (log A = 15.44) for KerPyr and

DOI: 10.1021/acs.energyfuels.7b00610
Energy Fuels 2017, 31, 6777−6781

Ker samples, respectively, and the values calculated by the OFW method are 249.5 ± 14.2 (log A = 15.09) and 237.6 ± 4.5 (log A = 14.46) for KerPyr and Ker samples, respectively. Thus, effective kinetic parameters of pyrolysis are uninfluenced by the significant amount of inherent pyrite presented in the kerogen of Bazhenov shale.

4. CONCLUSION

Isolation of kerogen demands monitoring of both structural and morphological parameters of the organic matter that can be reached by applying physical methods, including IR and solid-state NMR spectroscopies, SEM, and physisorption analysis. We showed that the pyrite removal procedure based on chromium(II) chloride treatment brings minimal changes in the structure and morphology of kerogen. Non-isothermal kinetic analysis of the obtained kerogen samples of Bazhenov shale revealed that the presence of inherent pyrite has no impact on the pyrolysis of the kerogen of Bazhenov shale. It should be kept in mind that in current study kerogen contains large grains of pyrite with low SSA. We think in case of pyrite particles with well-developed surface their influence on pyrolysis might be more pronounced.

AUTHOR INFORMATION

Corresponding Author

*E-mail: and_galuhin@mail.ru.

ORCID

Andrey Galukhin: 0000-0003-3077-3816

Notes

The authors declare no competing financial interest.

ACKNOWLEDGMENTS

The work was supported by Grant 14.Y26.31.0019 from the Ministry of Education and Science of Russian Federation.

REFERENCES

(1) International Energy Agency (IEA). *World International Outlook 2010*; IEA: Paris, France, 2010.
(2) Sarathi, P. S. *In-Situ Combustion Handbook: Principles and Practices*; National Petroleum Technology Office: Tulsa, OK, 1999; DOI: 10.2172/3175.
(3) Sunggyu, L.; Speight, J. G.; Loyalka, S. K. *Handbook of Alternative Fuel Technologies*; CRC Press: Boca Raton, FL, 2007.
(4) Williams, P. T.; Ahmad, N. *Appl. Energy* **2000**, *66*, 113−133.
(5) Wilson, A.; Lambert, D. E.; Collin, P. J. *Fuel* **1985**, *64*, 1647−1654.
(6) Allred, V. D. *Chem. Eng. Prog.* **1966**, *62*, 8.
(7) Braun, R. L.; Rothman, A. J. *Fuel* **1975**, *54*, 129−131.
(8) Ballice, L. *Fuel Process. Technol.* **2005**, *86*, 673−690.
(9) Al-Harahsheh, M.; Al-Ayed, O.; Robinson, J.; Kingman, S.; Al-Harahsheh, A.; Tarawneh, K.; Saeid, A.; Barranco, R. *Fuel Process. Technol.* **2011**, *92*, 1805−1811.
(10) Aboulkas, A.; El Harfi, K. *J. Fuel Chem. Technol.* **2009**, *37*, 659−667.
(11) Gai, R.; Jin, L.; Zhang, J.; Wang, J.; Hu, H. *J. Anal. Appl. Pyrolysis* **2014**, *105*, 342−347.
(12) Bakr, M.; Akiyama, M.; Yokono, T.; Sanada, Y. *Energy Fuels* **1991**, *5*, 441−444.
(13) Combaz, A. In *Kerogen: Insoluble Organic Matter from Sedimentary Rocks*; Durand, B., Ed.; Editions Technip: Paris, France, 1980.
(14) Robinson, W. E. *Organic Geochemistry, Methods and Results*; Eglinton, G., Murphy, M. T. J., Eds.; Springer: Berlin, Germany, 1969.
(15) Kontorovich, A. E.; Moskvin, V. I.; Bostrikov, O. I.; Danilova, V. P.; Fomin, A. N.; Fomichev, A. S.; Kostyreva, E. A.; Melenevsky, V. N. *Pet. Geosci.* **1997**, *3*, 343−358.
(16) Ulmishek, G. F. *Petroleum Geology and Resources of the West Siberian Basin, Russia*; U.S. Geological Survey: Reston, VA, 2003; U.S. Geological Survey Bulletin 2201-G, pp 49.
(17) Acholla, F.; Orr, W. *Energy Fuels* **1993**, *7* (3), 406−410.
(18) Taylor, P.; Evangelou, V. P. B.; Zhang, Y. L. *Crit. Rev. Environ. Sci. Technol.* **2009**, 37−41.
(19) Fathinia, S.; Fathinia, M.; Rahmani, A. A.; Khataee, A. *Appl. Surf. Sci.* **2015**, *327*, 190−200.
(20) Clough, A.; Sigle, J. L.; Jacobi, D.; Sheremata, J.; White, J. L. *Energy Fuels* **2015**, *29*, 6370−6382.
(21) Pugh, C.; Hossner, L.; Dixon, J. *Soil Sci. Soc. Am. J.* **1981**, *45*, 979−982.
(22) Kok, M. V.; Gundogar, A. S. *Fuel Process. Technol.* **2013**, *116*, 110−115.
(23) Galukhin, A.; Khelkhal, M. A.; Gerasimov, A.; Biktagirov, T.; Gafurov, M.; Rodionov, A.; Orlinskii, S. *Energy Fuels* **2016**, *30*, 7731−7737.
(24) Varfolomeev, M. A.; Nagrimanov, R. N.; Galukhin, A. V.; Vakhin, A. V.; Solomonov, B. N.; Nurgaliev, D. K.; Kok, M. V. *J. Therm. Anal. Calorim.* **2015**, *122*, 1375−1384.
(25) Varfolomeev, M. A.; Galukhin, A.; Nurgaliev, D. K.; Kok, M. V. *Fuel* **2016**, *186*, 122−127.
(26) Hong, Y.; Fegley, B., Jr. *Ber. Bunsenges. Phys. Chem.* **1997**, *101*, 1870−1881.
(27) Jablonski, A. E.; Lang, A. J.; Vyazovkin, S. *Thermochim. Acta* **2008**, *474*, 78−80.
(28) Ferdosian, F.; Yuan, Z.; Anderson, M.; Xu, C. C. *J. Anal. Appl. Pyrolysis* **2016**, *119*, 124−132.
(29) Vyazovkin, S. *Isoconversional Kinetics of Thermally Stimulated Processes*; Springer: Cham, Switzerland, 2015; DOI: 10.1007/978-3-319-14175-6.
(30) Ozawa, T. A. *Bull. Chem. Soc. Jpn.* **1965**, *38*, 1881−1886.
(31) Flynn, J. H.; Wall, L. A. *J. Polym. Sci., Part B: Polym. Lett.* **1966**, *4*, 323−328.
(32) Friedman, H. L. *J. Polym. Sci., Part C: Polym. Symp.* **1964**, *6*, 183−195.

DOI: 10.1021/acs.energyfuels.7b00610
Energy Fuels 2017, 31, 6777−6781